Time-lapse acquisition with a dual-sensor streamer over a conventional baseline survey

Anthony Day,* Martin Widmaier, Torben Høy and Berit Osnes, PGS, describe an experiment to validate the use of a dual-sensor streamer for time-lapse acquisition.

A time-lapse 3D project involves repeat 3D seismic surveys over a producing hydrocarbon reservoir targeted towards identifying changes in the physical state of the reservoir arising from production. Such time-lapse surveys are used to optimize the planning of producer and injector well placement. The first survey is the baseline survey, and each successive survey is a monitor survey. Ideally, the acquisition geometry and hardware is repeated exactly from survey to survey, as are environmental conditions, such that any observable difference is derived entirely from physical changes in the reservoir state. Variations in acquisition geometry naturally invoke variations in target illumination, and variations in wavefield sampling, and will contribute errors to the time-lapse signal. Variations in acquisition hardware and/or environmental conditions will naturally invoke changes in the signal-to-noise content, signal fidelity, and the seismic wavelet, thus also contributing errors to the time-lapse signal.

For conventional marine acquisition employing towed streamers that record the pressure wavefield, the requirement to repeat the acquisition geometry means that all monitor surveys must be acquired at the same acquisition depth as the base survey. However, if a dual-sensor streamer is used, this requirement can be relaxed. Dual-sensor streamer technology allows the wavefield to be separated into up- and down-going parts, which may then be independently redatumed to emulate acquisition at any recording depth. Thus the streamer may be towed at any depth, which usually means that we choose a deeper towing depth than would be used for conventional acquisition in order to take advantage of the quieter recording environment and increase the data low-frequency content.

In order to validate this approach, a time-lapse acquisition experiment was conducted in the North Sea whereby dual-sensor streamer data were acquired over five adjacent lines that had been acquired earlier in the year using a conventional streamer. The data were then processed and analyzed using a modern time-lapse processing sequence. Given that only a few months had elapsed between baseline and monitor surveys and there had been no production in the area, we expect to observe minimal differences between the two datasets. This paper describes the results of this time-lapse experiment.

* *Corresponding author, E-mail: anthony.day@pgs.com*

Acquisition

The time-lapse repeatability trial was carried out in Quad 26 of the Norwegian North Sea. A 3D survey was acquired using conventional streamers that recorded the pressure wavefield at a depth of 8 m in April 2009. Although this survey was not specifically designed as a baseline survey for a time-lapse experiment, five adjacent sail lines were selected as the 'baseline' survey for the dual-sensor repeatability trial. These five sail lines were then reacquired using dual-sensor streamers towed at a depth of 15 m in June 2009. This acquisition represents the 'monitor' survey. Figure 1 shows the survey location including the position of the five test lines that were used in this repeatability experiment.

The acquisition parameters for the baseline and monitor surveys are summarized in Table 1. This table shows that the only difference between the acquisition geometry of the two surveys is the streamer type and depth. The source parameters were identical in every respect for the baseline and monitor surveys; not only was the source volume identical between the two surveys, but the gun type and positions were also matched.

The baseline survey acquisition was not tailored to the needs of time-lapse acquisition in that it was acquired with the aim of optimizing coverage rather than ease of repeatability. Nevertheless, the five lines that were used in the repeatability study were chosen for their moderate streamer feathering and shot positions that fall relatively close to a

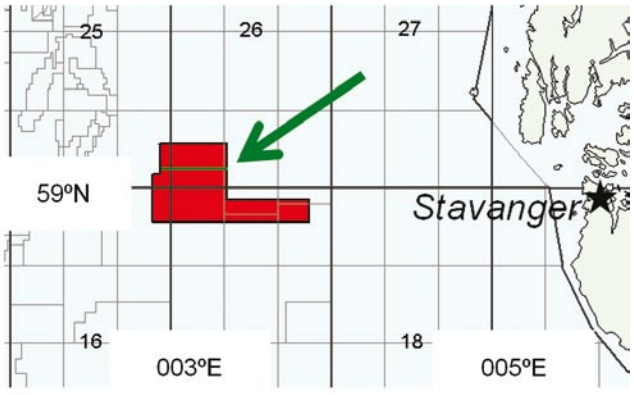

Figure 1 *Location of the survey area, with the five lines used for the repeatability experiment highlighted in green.*

	Baseline survey	Monitor survey
Vessel	Ocean Explorer	Atlantic Explorer
Streamer type	Conventional	Dual-sensor
Streamer depth	8 m	15 m
Number of streamers	6	6
Streamer length	5100 m	5100 m
Streamer separation	100 m	100 m
Source volume	3090 in^3, dual-source	3090 in^3, dual-source
Source depth	6 m	6 m
Survey date	April 2009	June 2009

Table 1 *Summary of the acquisition parameters for the baseline and monitor surveys.*

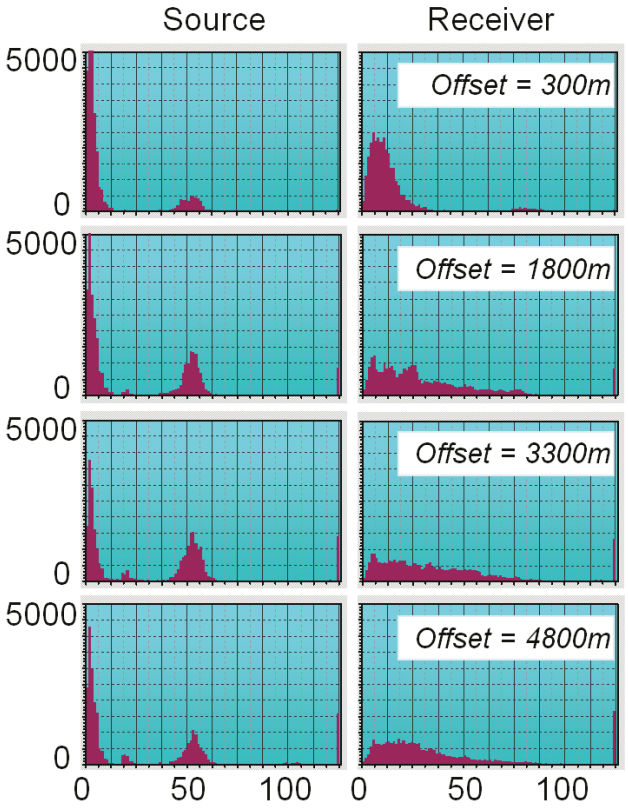

Figure 2 *Histograms of the minimum source distance (left) and receiver distance (right) in metres between base and monitor surveys after 4D binning.*

straight line to facilitate repetition of source and receiver positions. The monitor survey was acquired as a time-lapse survey whereby the source positions from the base survey were repeated. Acquisition was performed over a period of three days which was further limited by time-sharing constraints. Consequently, it was not possible to achieve optimal feather matching, although the source positions were matched well. This behaviour is illustrated by the minimum source and receiver distances after 4D binning as shown

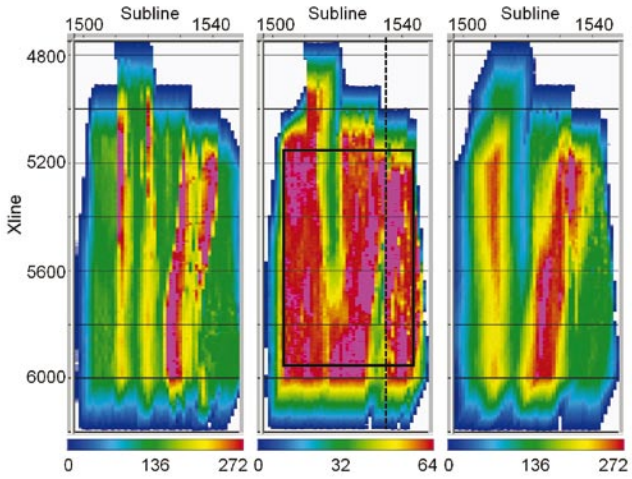

Figure 3 *Mid-offset fold of coverage maps for the baseline (left) and monitor (right) surveys. The result in the middle is the fold of the common baseline and monitor traces after 4D binning . The bold rectangle in the middle is the full fold area used for various analyses. The line for which stack comparisons are shown is also indicated (dashed line).*

in Figure 2. This figure demonstrates that the difference in source locations that were chosen for common traces in the 4D analysis are generally close to zero (except where traces from the alternative sources have been paired) whilst there is a much greater distribution of receiver location differences, especially at larger offsets. Despite these limitations, the baseline survey geometry was repeated sufficiently closely to permit meaningful time-lapse analysis. The resulting fold of coverage is summarized in Figure 3. The full fold area indicated in the central panel of Figure 3 was used to calculate time-lapse attributes, and example stack comparisons will be presented for the line indicated in this figure.

Processing

In order to perform time-lapse analysis, the baseline and monitor survey data, which were recorded at different depths, must be matched. The receiver depth controls the

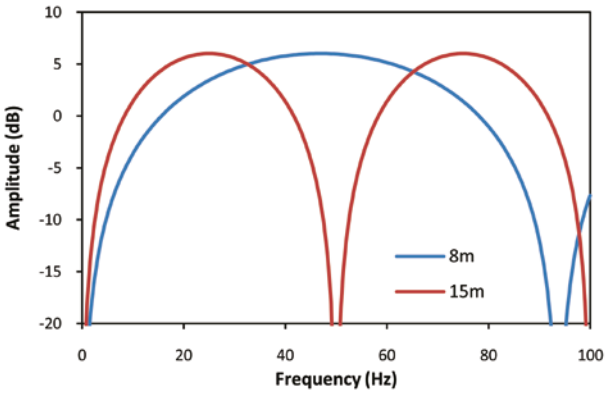

Figure 4 *Normal incidence amplitude spectra of the receiver ghost functions for 8 and 15 m recording depth.*

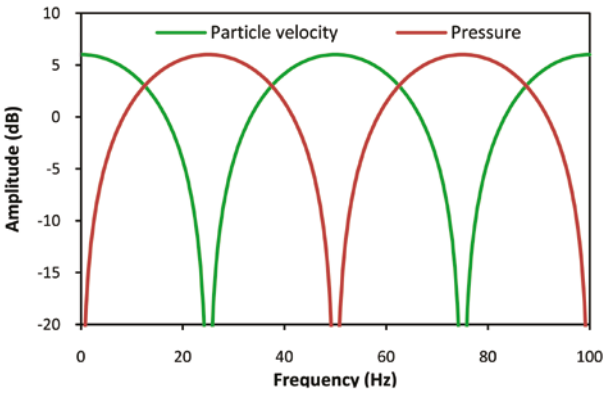

Figure 5 *Normal incidence amplitude spectra of the receiver ghost functions at 15 m recording depth for a pressure and particle-velocity sensor.*

time delay between primary energy and its ghost reflection from the sea surface on the receiver side. These ghosts give rise to 'notches' in the amplitude spectrum that represent frequencies at which the primary energy and its ghost destructively interfere, as illustrated in Figure 4 for 8 m and 15 m receiver depths. Wherever there is a notch in either the baseline or monitor survey data, the signal-to-noise ratio for this dataset will be very poor. Consequently any attempt to match the baseline and monitor survey data will be unstable near these frequencies, and there will be no contribution to the time-lapse signal wherever there is a notch in either of the datasets. Figure 4 shows that, for a 15 m streamer depth, a notch is introduced at ~50 Hz. Since we expect to record significant signal near this frequency in the North Sea, this streamer depth is inappropriate for time lapse acquisition over a baseline survey acquired at 8 m depth in this environment whenever conventional streamers are used.

A dual-sensor streamer contains collocated sensors that measure the pressure and vertical component of particle velocity. The frequency content of the signal recorded by the particle velocity sensor exactly complements that of the pressure sensor as illustrated in Figure 5. Hence, by combining the data from the two sensors we can circumvent the problem of low signal-to-noise at the notch frequencies that was outlined above. Standard processing of dual-sensor streamer data involves combining the measurements from the two sensors to separate the wavefield into up- and down-going parts, as described by Carlson et al. (2007). If we consider only the up-going wavefield, we have removed the receiver ghost reflection. However, in the case of the time-lapse experiment which is the subject of this paper, the baseline data contains a receiver ghost characteristic of the 8 m recording depth. Although it is possible to remove the receiver ghost for total pressure field data in isolation, subject to certain assumptions about the sea surface state, the results tend to suffer from poor signal-to-noise in the vicinity of the notch frequencies as described above and demonstrated by Tabti et al. (2009). Therefore, we prefer to process the dual-sensor data acquired at 15 m depth to determine the total pressure field at the acquisition depth of the conventional streamer data (8 m). This procedure is more robust and relies on fewer assumptions than removing the ghost from the conventional data, and is therefore likely to produce a superior time-lapse result.

The procedure by which the total pressure field at the recording depth of the baseline survey is reconstructed is illustrated by the schematic in Figure 6. For scattered energy returning from the earth, arrival time increases along the direction of the arrows in this figure. From this depiction, it is clear that, when redatuming from 15 m recording depth to 8 m depth, the up-going energy must be propagated forward in time whilst the down-going energy must be propagated backward in time. In practice this redatuming is implemented as a phase shift operator in the f-k domain that takes account of the changes in the required time shift with the emergence angle of the energy. After wavefield separation, the up- and down-going wavefields were independently redatumed from 15 m to 8 m depth, then summed to emulate the total pressure field that would have been recorded by conventional cables at 8 m depth. Since the up- and down-going energy

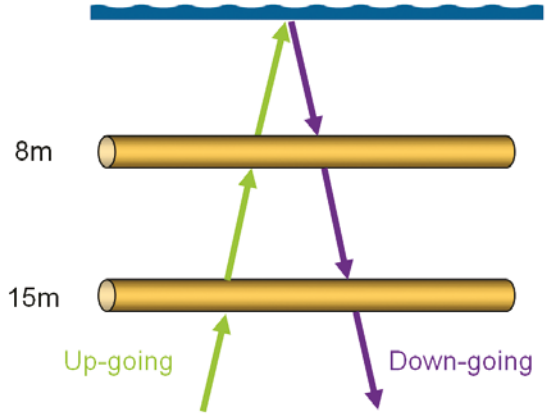

Figure 6 *Schematic representation of the procedure for reconstructing total pressure field data at a different datum level to the recording depth.*

must be treated differently in the redatuming step, wavefield separation is a necessary prerequisite for this matching operation, which is straightforward for dual-sensor data but cannot be achieved for conventional pressure data without introducing instability near the notch frequencies. The wavefield separation and redatuming approach correctly handles the amplitudes for all emergence angles and takes account of deviations from the nominal recording depth (Söllner et al., 2008). Furthermore, no distinction is made between primary and multiple energy: all multiples are separated from their receiver-side ghosts and recombined after redatuming just as for the primary energy. This flexibility allows us to tow the dual-sensor streamer at a greater depth than that used for the baseline survey in order to take advantage of the quieter noise regime, which would not be viable for a conventional streamer.

After reconstructing the total pressure field at 8 m acquisition depth, a deterministic matching filter was applied to correct for the differences in the instrument response of the recording filters used for the dual-sensor and conventional streamers. Both the baseline and monitor datasets were then taken through a modern time-lapse processing sequence as outlined in Table 2. Points of note concerning the processing sequence include the following:

- The tidal static correction is based on a measured tidal range plus a per-sail line residual static, which is required because the tidal measurements were taken well outside the survey array.
- The 4D binning step was based on a minimum source-receiver distance criterion only, and was used to replicate coverage holes in each of the two surveys.
- The 3D bin centre regularization includes interpolation of empty bins, which due to the 4D binning step are the same for both base and monitor survey.

Note that, although this is a modern time-lapse processing sequence, it was deliberately kept fairly simple since the primary purpose of this experiment was to validate the use of a dual-sensor streamer for time-lapse acquisition rather than to obtain the best possible time-lapse processing result. It is possible that an improved time-lapse result could be obtained with a careful effort to optimize the processing sequence for this particular dataset.

Results

In this section, we present the results of the time-lapse experiment by comparing the baseline and monitor data at different stages of the processing sequence. Given that the baseline and monitor surveys were conducted a few months apart in an area with no production, we anticipate that there should be minimal differences between the two surveys, i.e., the ideal result is perfect repeatability. The results are evaluated by showing the difference between the baseline and monitor survey results for stacks of a selected line and quantified using conventional time-lapse quality control attributes calculated for the entire full fold area.

Pre-processing	Noise attenuation (swell noise, direct and refracted energy)
	Wavefield reconstruction and instrument matching (monitor only)
	Zero-phasing
Pre-migration	Tau-p deconvolution (shot and receiver domains)
	2-D SRME (longer periods only)
	Tidal static correction
	Parabolic radon demultiple
	4-D binning
	3-D data regularization
Final	3-D pre-stack time migration
	Final global matching (design window 900-3000msecs)

Table 2 *Summary of the time-lapse processing sequence.*

Figure 7 shows a stack of an example subline after application of the pre-processing steps defined in Table 2. The strong reflector at ~1600 ms two-way time is the reflection from the top of the Cretaceous chalk body. Although there are no reservoirs in the area over which this time-lapse experiment was conducted, most reservoirs in this region can be found in the vicinity of this reflector. Hence, for the purposes of this exercise, the 'target of interest' is taken to be a window spanning this chalk reflector.

For the purposes of the comparison in Figure 7, the 4D binning step has been applied to equalize the fold in both sections, and the tidal static corrections have also been applied since these have been shown to have a significant impact on repeatability. Consequently, this figure represents the raw difference between the baseline and monitor surveys after minimal processing. Even at this early stage in the processing sequence, the difference between the baseline and monitor survey is observed to be very small.

The corresponding results after final processing are shown in Figure 8. As would be expected, the application of the full processing sequence outlined in Table 2 has further reduced the differences between the baseline and monitor survey. Differences are confined to the seafloor and the removal of the first water column multiple, where it is unrealistic to expect a perfect time-lapse result given the shallow water and the acquisition configuration that was employed. It is likely that the large cross-line emergence angles for very shallow reflectors, which are neglected in the wavefield separation and redatuming steps, are a contributory factor to these residuals. It has been shown that such effects can be mitigated by apply-

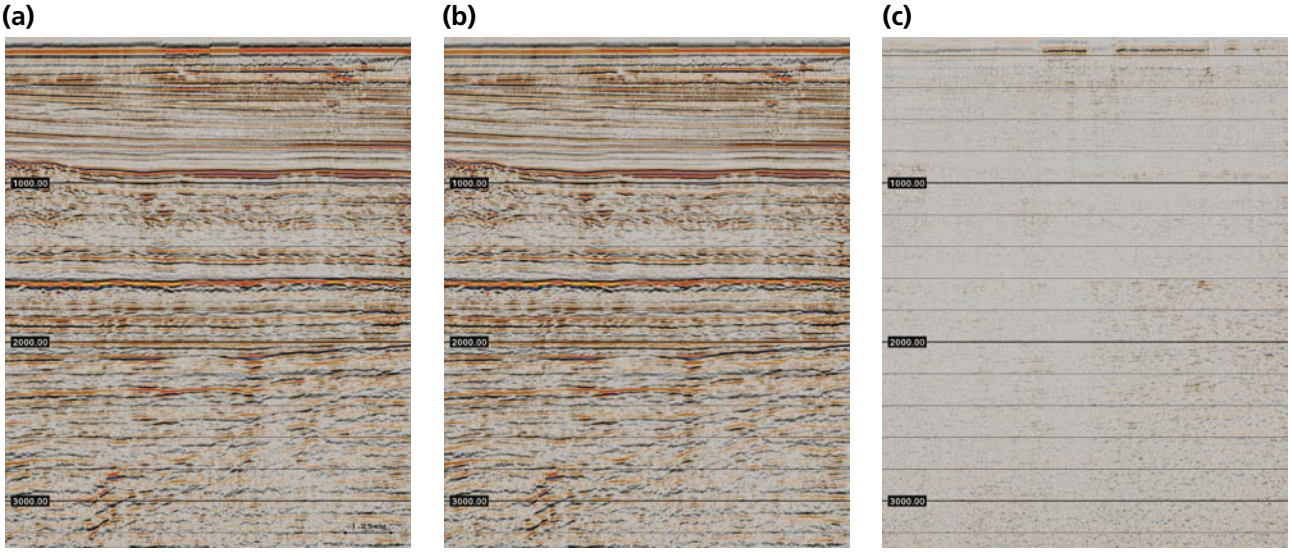

Figure 7 *Stack of a single sub-line after the pre-processing steps for a) the baseline and b) monitor surveys, and c) the difference between them.*

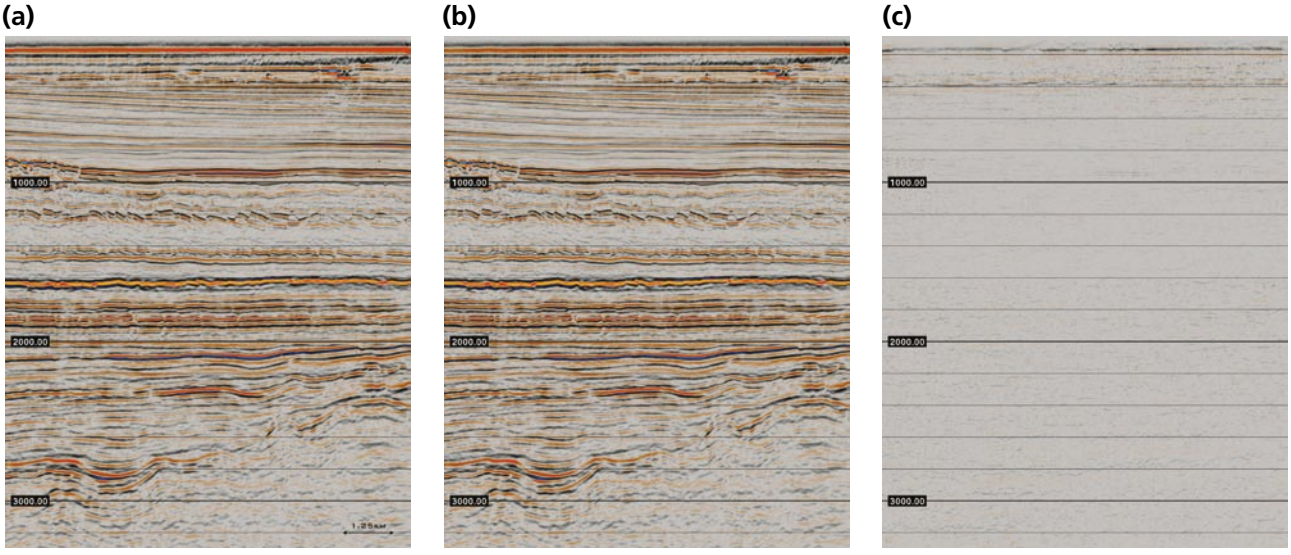

Figure 8 *Stack of a single sub-line after final processing a) for the baseline and b) monitor surveys, and c) the difference between them.*

ing a 3D wavefield separation after suitable data reconstruction (Klüver et al., 2009). However, this data example again demonstrates that 3D effects have negligible to zero influence on seismic data integrity and the time-lapse signal in typical target regions, so this step has been omitted.

Figure 9 shows comparative amplitude spectra for the baseline and monitor surveys after the pre-processing steps and for the final result. This figure further confirms the good quality of the match between the baseline and monitor surveys. In particular, the agreement at the pre-processing stage is similar to that which could be expected for time-lapse acquisition with conventional cables at the same depth as the baseline survey. Recall that pressure data recorded at 15 m depth has a notch at ~50Hz. This means that the signal for the monitor survey must be derived almost exclusively from the particle velocity sensor near this frequency. Hence the excellent match between the amplitude spectra for the baseline and monitor surveys at the pre-processing stage serves to validate the acquisition system and the processing sequence that has been used to emulate the conventional acquisition at 8 m recording depth: it would not be possible to achieve such a close match without good quality data from the velocity sensor or if the wavefield separation and redatuming procedures were fundamentally flawed.

In order to quantify the repeatability between the baseline and monitor, a number of time-lapse quality control attributes were calculated for the target interval after each major step in the processing sequence. Figure 10 shows the normalized RMS difference, cross-correlation, and time shift attributes after pre-processing, pre-migration and after

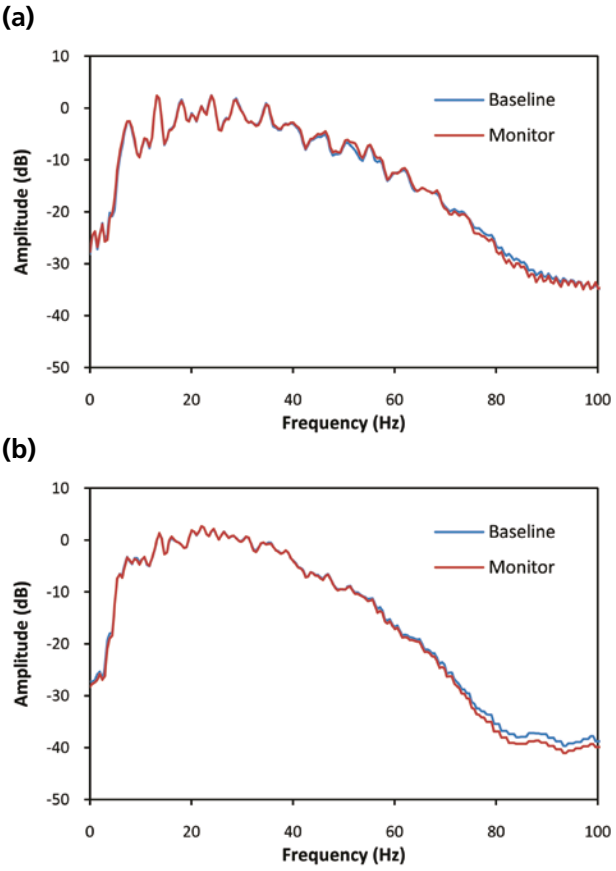

Figure 9 *Spectral comparison of the baseline and monitor surveys a) after pre-processing and b) final processing. The analysis window is 1300–2600 ms.*

final processing. The attributes are shown as maps of the full fold area. This figure demonstrates the improvement in the repeatability between baseline and monitor as the processing sequence progresses. At the pre-processing step, the time shift attribute shows a significant bias which has been removed later in the processing sequence, primarily due to the application of tidal static corrections.

The multiple suppression steps also significantly improve the repeatability, which is also thought to be in part due to tidal effects which give rise to different multiple periodicity for the baseline and monitor survey and contribute to reduced repeatability prior to multiple suppression. The migration and matching filter further improve the repeatability such that the normalized RMS difference after full processing is around 10%. This result is consistent with the repeatability that can be obtained using conventional streamers in this area, thereby validating the use of dual-sensor streamer technology for time-lapse acquisition.

All the results presented so far cover the full offset range. As a final check that the repeatability is good at all offsets, stacks were calculated for several reflection angle ranges. Figure 11 shows the difference stacks for these angle ranges compared to the full offset range for that part

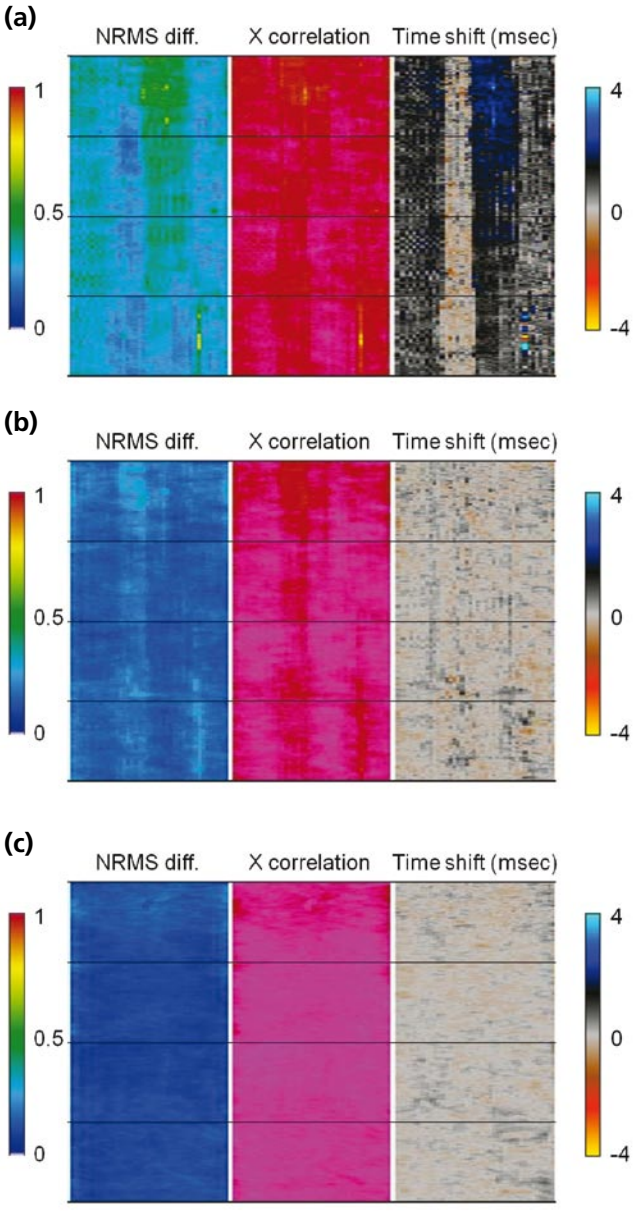

Figure 10 *Maps showing the normalized RMS difference, cross-correlation and time shift between the baseline and monitor surveys a) after pre-processing, b) pre-migration and c) final processing. Results have been calculated for an 800–1800 ms window over the full fold area. The colour scale on the left applies to both the normalized RMS difference and cross-correlation figures; the time shift scale is shown right in ms.*

of the data for which all the angle ranges have full fold. Whilst there is more noise in the difference stacks for the restricted angle ranges than the full offset range, which is expected due to the reduced fold, there is no evidence of any systematic differences in repeatability between the different angle ranges. This result serves to confirm that the processing applied to the dual-sensor streamer data has correctly reconstructed the total pressure field for all offsets.

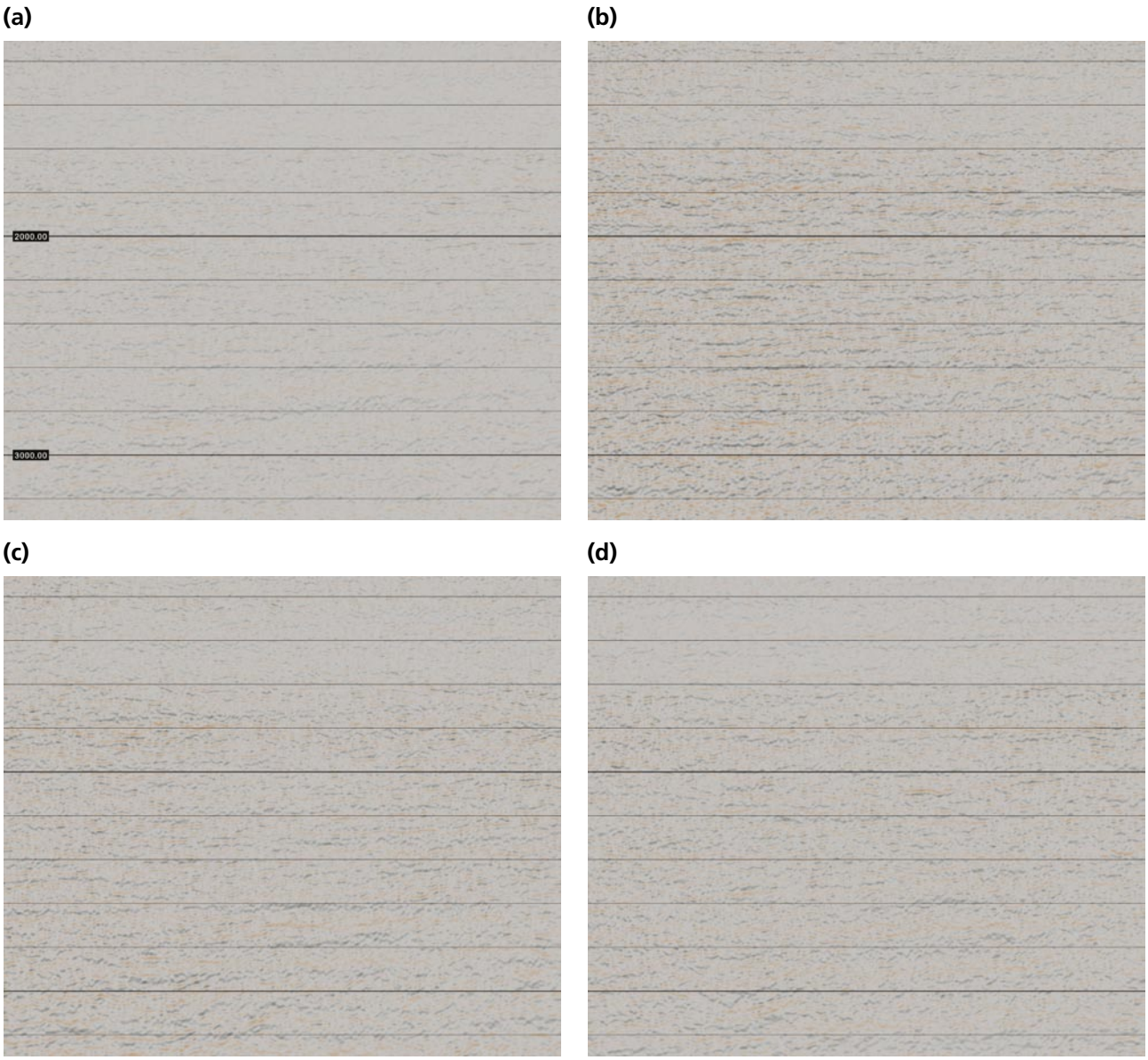

Figure 11 *Difference stacks in the full fold region for a) the full offset range and three different reflection angle ranges after final processing: b) 5.0-17.5°, c) 17.5-27.5° and d) 27.5-40.0°.*

Future time-lapse studies

In order to perform time-lapse processing, the baseline and monitor survey data must be matched. In practice, we can only expect to retrieve a reliable time-lapse signal in parts of the spectrum where both base and monitor survey have sufficiently good signal-to-noise ratio as discussed previously. In the example in this paper, we have been required to reintroduce the receiver ghost notch structure of the conventional baseline survey into the dual-sensor streamer data in order to perform time-lapse analysis. By doing so, we have deliberately degraded the data obtained from the dual-sensor streamer due to the limitations of the conventional data with which we wish to compare it.

If we consider the up-going pressure field, which is the usual output from dual-sensor streamer processing, we have removed the effects of the receiver-side ghost. We would therefore expect to obtain better resolved seismic data as a result of the increased bandwidth that follows from the removal of this ghost. This effect is illustrated in Figure 12 which shows the modelled vertical far-field signature for the source used to acquire the data in this paper. The source signature is shown both with and without a receiver ghost for 8 m streamer depth included, which clearly shows that the input source wavelet is lengthened by the presence of the ghost, thereby degrading resolution. The zero-phase equivalents of these two wavelets are also shown since

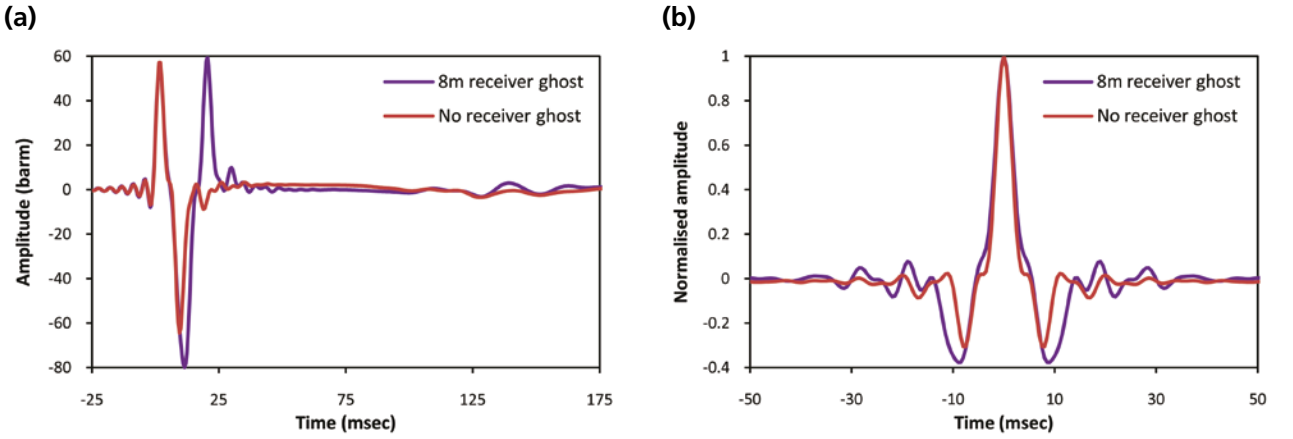

Figure 12 *a) Vertical far-field signature for the seismic source used in this time-lapse experiment with and without the receiver ghost for 8 m recording depth, and b) the zero phase equivalents . The zero phase wavelets have been normalized to the same maximum amplitude.*

a zero-phasing filter is applied early in the processing sequence. After this step, the reduced resolution that follows from the presence of the ghost manifests as higher amplitude side lobes surrounding the central peak of the wavelet.

In order to demonstrate this effect on the data example shown in this paper, the up-going pressure field was determined from the dual-sensor streamer data and processed using the same sequence as used for the time-lapse analysis. Figure 13 compares the final images obtained from the up-going pressure field and the emulated total pressure field at 8 m recording depth, both of which were obtained from the dual-sensor streamer data. These images have been scaled such that the central peak of the wavelet for the top chalk reflector at ~1600 ms two-way time has approximately the same amplitude. Inspection of these images demonstrates the higher amplitude side lobes in the zero-phase wavelet in the presence of the receiver ghost. Whilst the amplitude of these side lobes might not affect the gross structural interpretation of the seismic images in this case, the larger side lobes when the receiver ghost is present will degrade the resolution of fine detail which might be critical for accurate reservoir interpretation. Figure 14 shows comparative amplitude spectra for the data in Figure 13 which demonstrates that the up-going pressure field has broader bandwidth than the total pressure field data, which reflects the enhanced resolution seen in the seismic images.

This example serves to illustrate the data quality advantages that follow from removing the effect of the receiver-side ghost. It follows that time-lapse analysis will also benefit if both baseline and monitor surveys were acquired using technology that permits the removal of this ghost, such as the dual-sensor streamer. If the ghost could be removed from both datasets, there would no longer any need to degrade one dataset to replicate the limitations of the other. Time-lapse analysis could thus be performed over a broader bandwidth, and it would be expected that more reliable estimates of the

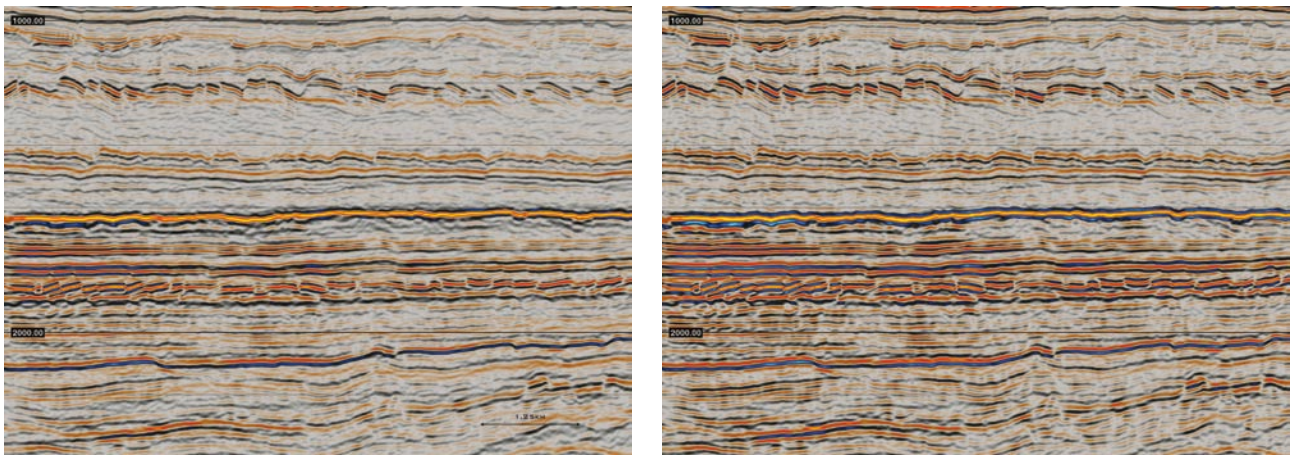

Figure 13 *a) Final image obtained from the dual-sensor streamer data for the up-going pressure field and b) the total pressure field emulated for 8 m streamer depth.*

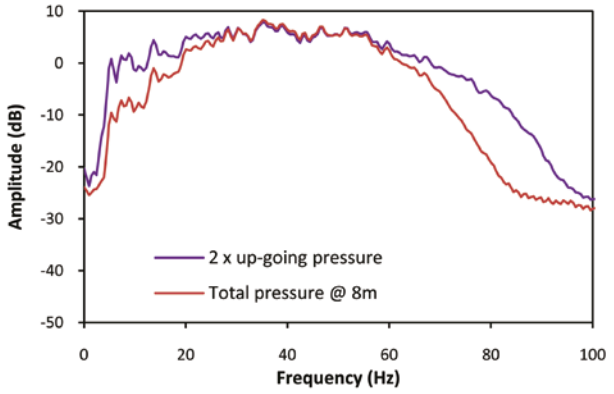

Figure 14 *Comparative amplitude spectra for the final images shown in Figure 13 for an analysis window from 1300–2600 ms.*

time-lapse attributes would be obtained. Furthermore, when a true wavefield decomposition is performed, as is possible for dual-sensor streamer data, the receiver-side effects of the rough sea-surface are eliminated since they are confined to the down-going pressure field after suitable multiple suppression. This effect could potentially further improve time-lapse repeatability since rough sea surface effects have been shown to degrade time-lapse repeatability (e.g., Laws and Kragh, 2002).

Conclusions

A time-lapse experiment was carried out in the North Sea whereby a 'monitor' survey was acquired using dual-sensor streamers at 15 m depth over a 'baseline' survey that had been acquired a few months earlier using conventional streamers at 8 m depth. Wavefield separation was performed for the dual-sensor streamer data and the up- and down-going pressure fields independently redatumed from 15 m to 8 m depth and summed to emulate the total pressure field acquired using the conventional streamer. The data were then processed using a modern time-lapse processing flow. The differences between the two datasets were found to be minimal as expected given that there was no production in the survey area during the months between the two surveys. Time-lapse attributes were calculated in order to quantify the repeatability. These attributes demonstrate that the final results are consistent with the results that can be obtained using conventional streamers in this area, with a final normalized RMS difference in the target area of 10%. This result demonstrates that a dual-sensor streamer can be used to acquire time-lapse monitor surveys over baseline surveys acquired using conventional streamers with high repeatability, and further serves to validate the integrity of the wavefield separation and redatuming steps applied to the dual-sensor streamer data. However, in order to obtain this result it was necessary to reintroduce a receiver-side ghost corresponding to the recording depth of the baseline survey into the dual-sensor streamer data due to the limitations of the conventional streamer data. In the future, the full benefit of the increased bandwidth for time-lapse surveys will only be realized when both baseline and monitor surveys are acquired with technology that permits the removal of the effects of the receiver-side ghost, such as the dual-sensor streamer.

Acknowledgments

We thank the crews of the *Ocean Explorer* and *Atlantic Explorer* who acquired the data used in this study, Berit Mattson and Zbigniew Greplowski for their contributions to processing the data, and also PGS for permission to publish this paper.

References

Carlson, D., Long, A., Söllner, W., Tabti, H., Tenghamn, R. and Lunde, N. [2007] Increased resolution and penetration from a towed dual-sensor streamer. *First Break*, **25**(12), 71-77.

Klüver, T., Aaron, P., Carlson, D., Day, A. and van Borselen, R. [2009] A robust strategy for processing 3D dual-sensor towed streamer data. *SEG*, Expanded Abstracts 28, 3088-3092.

Laws, R. and Kragh, E. [2002] Rough seas and time-lapse seismic. *Geophysical Prospecting*, **50**, 195-208.

Söllner, W., Day, A. and Tabti, H. [2008] Space-frequency domain processing of irregular dual-sensor towed streamer data. *SEG*, Expanded Abstracts 27, 1078-1082.

Tabti, H., Day, A., Schade, T., Lesnes, M. and Høy, T. [2009] Conventional versus dual-sensor streamer deghosting: a case study from a Haltenbanken survey. *First Break*, **27**(8), 101-108.